Eu^{2+}-doped NaCl crystals exposed under the same conditions we could virtually exclude the existence of detectable quantities of the Suzuki phase as the intensities of reflections induced by the second harmonic wavelength were exactly the same for both materials.

In Eu^{2+}-doped NaCl crystals the precipitation results in two phases (*A* and *B*) differing in crystal structure, distribution in the host lattice and thermal stability. The crystal structure of the more stable phase *A* has been determined and described in this paper. $EuCl_2$ precipitating in the NaCl host lattice crystallizes in the fluorite type of structure contrary to pure $EuCl_2$ crystallizing in the $PbCl_2$ structure (Doll & Klemm, 1939). It appears that under these conditions a new polymorphic modification of $EuCl_2$, perhaps contaminated by Na, can exist. Eu–Cl in this structure is equal to 3·02 Å, in good agreement with the Goldschmidt atomic radii 1·24 and 1·81 Å of Eu^{2+} and Cl^-, respectively.

Phase *B* was found to nucleate at subgrain boundaries in the vicinity of which strong distortion of the host lattice can be expected. This fact supports our speculative as well as unexpected assignment to the *Pm3m* space group and $EuCl_2.2NaCl$ formula. Moreover, considerably lower thermal stability of phase *B* (in comparison with phase *A*) is also in accord with the presence of charge-compensating cation vacancies facilitating the diffusion of Eu^{2+} ions and dissolution in the host matrix. It should also be noticed that phase *B* undergoes a continuous destruction under the action of X-ray photons rendering it difficult to obtain the number of data necessary for a structure determination.

References

DOLL, W. & KLEMM, W. (1939). *Z. Anorg. Allgem. Chem.* **241**, 239–258.

International Tables for X-ray Crystallography (1974). Vol. IV. Birmingham: Kynoch Press.

JEHANNO, G. & PERIO, P. (1968). *Bull. Soc. Fr. Minéral. Cristallogr.* **91**, 5–9.

LEVELUT, A. M., LAMBERT, M. & GUINIER, A. (1968). *Acta Cryst.* A**24**, 459–464.

LILLEY, E. & NEWKIRK, J. B. (1967). *J. Mater. Sci.* **2**, 567–582.

LOON, C. J. J. VAN & IJDO, D. J. W. (1974). *Acta Cryst.* B**31**, 770–773.

MIYAKE, S. & SUZUKI, K. (1954). *J. Phys. Soc. Jpn*, **9**, 702–712.

NORTH, A. C. T., PHILLIPS, D. C. & MATHEWS, F. S. (1968). *Acta Cryst.* A**24**, 351–359.

SORS, A. J. & LILLEY, E. (1975). *Phys. Status Solidi A*, **32**, 533–539.

STĘPIEŃ-DAMM, J., MUGEŃSKI, E. & ŁUKASZEWICZ, K. (1978). *Acta Cryst.* A**34**, S245.

SUZUKI, K. (1955). *J. Phys. Soc. Jpn*, **10**, 794–804.

SUZUKI, K. (1961). *J. Phys. Soc. Jpn*, **16**, 67–78.

SWAMY RAO, K. N. & PARASNIS, A. S. (1977). *Philos. Mag.* **36**, 265–278.

TOMAN, K. (1963). *Czech. J. Phys.* B**13**, 269–301.

VLASAK, G. & HARTMANOVA, H. (1975). *Krist. Tech.* **10**, 369–373.

VOSZKA, R., TARJAN, I., BERKES, L. & KRAJSOVSZKY, J. (1966). *Krist. Tech.* **1**, 423–426.

X-RAY 70 system. Tech. Rep. TR-192. Computer Science Centre, Univ. of Maryland, College Park, Maryland.

YACAMAN, M., HOBBS, L. W. & GORINGE, M. J. (1977). *Phys. Status Solidi A*, **39**, K85–K90.

Acta Cryst. (1980). A**36**, 57–67

The Scattering of High-Energy Electrons. II. Quantitative Validity Domains of the Single-Scattering Approximations for Organic Crystals

BY BING K. JAP* AND ROBERT M. GLAESER

Division of Medical Physics and Donner Laboratory, University of California, Berkeley, California 94720, *USA*

(*Received* 28 *March* 1979; *accepted* 2 *August* 1979)

Abstract

Two approximations that are commonly used to describe the scattering of high-energy electrons are the first Born approximation (kinematic approximation) and the closely related 'weak phase-object' approximation. The quantitative domains of validity for the use of these two scattering approximations for structural analysis of organic crystals are evaluated numerically in terms of resolution, crystal thickness and incident electron energy. The resulting calculations show how

* Present address: Department of Physics, University of Alberta, Edmonton, Alberta, Canada.

0567-7394/80/010057-11$01.00

progressively important dynamical scattering effects lead to an increasingly large contribution to the R value in a structure factor analysis. Alternatively, the results show that an increasing dissimilarity is produced between the structure inferred from electron microscope images and the correct structure. The results also show that the actual images (and the structure inferred from the images) remain qualitatively similar to the projected Coulomb potential, even though dynamical scattering effects may lead to a large *quantitative* dissimilarity relative to the correct structure.

1. Introduction

The so-called kinematic approximation (first Born approximation) and the closely-related 'weak phase-object' approximation are aptly described as single-scattering approximations since they are first order in the scattering potential. These two single-scattering approximations are most attractive for structural analysis in electron microscopy because the transmitted wave function for a given object is linearly related to the object structure. This linearity provides the important property that the approximations are *invertible*, in the sense that the object structure can be retrieved directly from the transmitted wave function. With the use of appropriate imaging conditions, the transmitted wave function can be determined from the electron microscope image intensities (see, for example, Hoppe, Langer & Thon, 1970; Erickson & Klug, 1971; Frank, 1972; Stroke & Halioua, 1973*a*,*b*).

The validity domains (for obtaining an agreement with experimental images) of single-scattering approximations, in particular the weak phase-object approximation, have been recently given by Lynch, Moodie & O'Keefe (1975). Their study was concerned with an inorganic crystal and was limited to an electron energy of 100 keV. Jefferson, Millward & Thomas (1976) have recently studied the validity of the weak phase-object approximation for the interpretation of lattice fringes of graphite. Their calculations demonstrate that the weak phase-object approximation fails to describe correctly the appearance of lattice fringes (exact Bragg condition) for a specimen thickness of 40 to 100 Å. It is important to note here that the weak phase-object approximation is a high-energy limit of the kinematic approximation, and its failure in the correct interpretation of lattice fringes does not conclusively imply the failure of the kinematic approximation itself, and thereby the importance of dynamical scattering effects. A brief comparison of the results obtained with the weak phase-object approximation, the kinematic approximation and the multislice method has also been reported by Ishizuka & Uyeda (1977) for the case of a rather complex organometallic crystal structure, copper hexadecachlorophthalocyanine.

In this paper, the domains of validity of the two single-scattering formulations for structural analysis of organic crystals are evaluted for different incident electron energies. In the evaluation, the multislice dynamical formulation of Cowley & Moodie (1957) is assumed to give the 'exact' transmitted wave function, which can be used as our standard of reference. Only the elastically scattered electrons from a perfect single crystal are considered. The inelastic scattering effects, including the effect of thermal diffuse scattering, have been ignored in order to simplify the calculation. These effects could be described phenomenologically as the contribution arising from an 'imaginary potential'.

2. The test objects

Two different organic crystals, anhydrous cytosine and disodium 4-oxypyrimidine-2-sulfinate hexahydrate, were used as our test objects for the evaluation of the validity of the single-scattering approximations. These crystals differ not only in their structures but also significantly in their unit-cell dimensions. The difference in unit-cell dimensions results in a different number of beams being strongly excited. The use of two different crystals can show, therefore, the extent to which our evaluation of the validity of the invertible approximations depends upon the number of interacting beams, and upon other specific features.

(*a*) *The crystal structure of anhydrous cytosine*

The structure of anhydrous cytosine $C_4H_5N_3O$ has been previously determined by X-ray crystallography (Barker & Marsh, 1964). The crystals are orthorhombic with space group $P2_12_12_1$. The unit-cell dimensions are $a = 13{\cdot}041$, $b = 9{\cdot}404$ and $c = 3{\cdot}815$ Å.

(*b*) *The crystal structure of disodium 4-oxypyrimidine-2-sulfinate hexahydrate ('DISOPS')*

The crystal structure of 'DISOPS', $Na_2.C_4H_2N_2O_3S.6H_2O$, has been previously determined by X-ray analysis (Sletten, 1969). The crystals are orthorhombic with space group *Pcbm*. The unit-cell dimensions are $a = 9{\cdot}299$, $b = 20{\cdot}253$ and $c = 6{\cdot}946$ Å.

3. Method of calculation for the diffracted wave function

The first step in the computation of the diffracted wave function is to calculate the Fourier spectrum of the projected crystal potential. In all calculations reported here the direction of the projection was taken parallel to the

crystal c axis. The Fourier spectrum of the projected potential (c axis) for an orthorhombic structure can be represented by the following equations:

$$F(h,k) = \sum_{j=1}^{n} f_j(h/a, k/b) \exp 2\pi i(\mathbf{s}.\mathbf{r}_j); \quad (1a)$$

$$\bar{s} = h(\mathbf{a}/a^2) + k(\mathbf{b}/b^2); \quad (1b)$$

where $F(h,k)$ is the Fourier coefficient for the projected potential; (h,k) are Miller indices; f_j and $\mathbf{r}_j$ are, respectively, the form factor and the position of the jth atom in the crystal with unit-cell vectors **a**, **b** and **c** and n is the number of atoms in the unit cell. The Fourier coefficients for the projected potential were calculated to a spatial frequency of 2·0 Å^{-1}, and all of these coefficients were included in generating the projected potentials for subsequent multislice calculations.

The atomic form factor used was obtained from its representation as the sum of analytic functions with parameters determined by the type of atom. These parameters were tabulated by Doyle & Turner (1968) through curve fitting with values determined numerically using the relativistic Hartree–Fock atomic fields. The form factor for hydrogen was obtained by linear interpolation of values given in *International Tables for X-ray Crystallography* (1968).

(*a*) *Kinematic approximation*

In the kinematic approximation, the diffracted wave function from a finite parallel slab of crystal can be described by

$$F_{\text{kin}}(h,k) = -i\sigma F(h,k) H[\sin \pi\xi(h,k)\, H]/\pi\xi(h,k)\, H,$$
$$\xi(h,k) = (\lambda/2)\,(h^2/a^2 + k^2/b^2), \quad (2)$$

where $F_{\text{kin}}(h,k)$ is the diffracted wave function, σ is the electron interaction constant ($1/\hbar v$), $\xi(h,k)$ is the excitation error for the h,k reflection (orthorhombic lattice), λ is the electron wavelength, H is the crystal thickness and all other parameters have been defined previously. We have assumed that the amplitudes of the scattered beams for all crystal thicknesses are very small when compared to unity. We have also assumed that the electron wavelength is so small that the Ewald sphere does not come close to intersecting more than one reciprocal-lattice plane. This condition assumes that the upper layer lines will make only a negligible contribution to F_{kin}, as it is defined above.

(*b*) *Weak phase-object approximation*

In the high-energy limit, the transmitted wave function for the kinematic approximation takes the following simple form:

$$\psi_{\text{WP}}(x,y) = 1 - i\sigma\varphi(x,y)\, H, \quad (3)$$

where $\psi_{\text{WP}}(x,y)$ is the transmitted wave function, and $\varphi(x,y)$ is the object potential energy projected along the z axis. Equation (3) can also be derived as the first term in a power-series expansion of the phase-object approximation, $\exp[-i\sigma\varphi(x,y)H]$. The phase-object approximation, in turn, is exact in the high-voltage limit (Jap & Glaeser, 1978). The weak phase-object representation of the transmitted wave function has been widely used for the qualitative interpretation of electron scattering by thin objects (see, for example, Cowley & Jap, 1976) and is often called the weak phase-object approximation. This approximation assumes that the Ewald sphere is flat; the shape transform for the specimen thickness and the phase factor for Fresnel propagation are neglected. For thin objects or for very high electron energy, the approximation becomes an excellent representation of the kinematic approximation. At low electron energy and for thick objects, the weak phase-object approximation gives overestimated values for the diffracted intensities at high spatial frequencies, as will be seen below.

(*c*) *Multislice dynamical formulation*

The transmitted wave function in the multislice dynamical approximation can be described by the following recursive relationship:

$$\psi_n(x,y) = \left[\psi_{n-1}(x,y) * \exp\left(\frac{2\pi i}{\lambda}\frac{x^2+y^2}{2\Delta z_n}\right)\right] \times \left(\exp\frac{-i}{\hbar v}\int_{z_{n-1}}^{z_{n-1}+\Delta z_n} V(x,y,z)\,\mathrm{d}z\right), \quad (4)$$

where the symbol * denotes the convolution product. $\psi_{n-1}(x,y)$ and $\psi_n(x,y)$ are, respectively, the transmitted wave function after passing through a sequence of $(n-1)$ and n slices, Δz_n is the thickness of the nth slice, $V(x,y,z)$ is the crystal potential energy and λ is the electron wavelength. The diffracted wave function is the Fourier transform of the transmitted wave function, and can be represented by (Allpress, Hewat, Moodie & Sanders, 1972)

$$Q_n(h,k) = \mathscr{F}\left\{\exp\left[-\frac{i}{\hbar v}\int_{z_{n-1}}^{z_{n-1}+\Delta z_n} V(x,y,z)\,\mathrm{d}z\right]\right\};$$

$$\varphi_n(h,k) = \left\{\varphi_{n-1}(h,k) \times \exp\left[-i\pi\lambda\Delta z_n\left(\frac{h^2}{a^2}+\frac{k^2}{b^2}\right)\right]\right\} * Q_n(h,k), \quad (5)$$

where $\varphi_n(h,k)$ is the diffracted wave that would be obtained after passing through a sequence of n slices, $Q_n(h,k)$ is the diffracted wave function for the nth slice, $\mathscr{F}$ represents Fourier transformation, a and b are crystal constants (orthorhombic lattice) and * indicates the

convolution operation. For a crystalline object, the diffracted wave function can be represented by a set of Dirac delta functions while the transmitted wave function forms a spatially continuous function. For computational purposes, it is less time consuming to evaluate the diffracted wave function than the transmitted wave function, when the number of beams included is not large. For large unit-cell crystals, such as protein crystals, there is no advantage in evaluating the diffracted wave rather than the transmitted wave function.

The accuracy of the diffracted wave function evaluated according to (5) depends upon the choice for the thickness of the slice, as well as upon the number of beams included in the calculation. The slice thickness (Δz) used in the calculation should not, in principle, be so large that the Ewald sphere comes close to intersecting the reciprocal-lattice plane defined by the condition $s_z = 1/\Delta z$ at or before the resolution cut-off of the calculations. The so-called upper layer-line effect arises when the Ewald sphere comes close to intersecting this reciprocal-lattice plane. In our calculations, the slice thickness was taken to be identical with the short crystal-repeat distance. Calculations for DISOPS were also checked at 100 keV, using half the c axis distance as the slice thickness, to confirm that upper layer-line effects were not present.

For a given slice thickness, the computation should include as many diffracted beams as possible. If an insufficient number of beams is used, the total diffracted beam intensities diminish rapidly after passing through a number of slices. This occurs because a significant fraction of the electron energy becomes associated with those higher-order reflections, which are systematically neglected in the calculation.* With increasing crystal thickness, the accuracy of the computed wave function decreases when a limited number of beams are included. The conservation of the total diffracted-beam intensities can, therefore, reflect the accuracy of the computation. For our test objects, 739 and 922 reflections were included, respectively, for cytosine and for DISOPS. The total diffracted beam intensities decreased by a few per cent for crystal thickness up to 500 Å. At 100 keV for example, the total beam intensities for both crystals decreased by less than 1% at a crystal thickness of 100 Å. This percentage error decreases as the electron energy increases.

* Only those reflections which fall within a circle of desired radius are included. The number of reflections used is therefore much smaller than the two-dimensional array size that is used in the Fourier transform which generates the diffracted beams from the transmitted wave function of the first slice. The transmitted wave is not a band-limited function and, furthermore, the reflections having spatial frequencies larger than the band limit of $F(h,k)$ may, according to the Shannon sampling theorem (Goodman, 1968), be expected to have incorrect values. A recent paper of Ishizuka & Uyeda (1977) appears to include all reflections in their two-dimensional arrays in the calculation of the diffracted wave. This is, therefore, contrary to the criterion set forth by the sampling theorem regarding the minimum sampling interval.

4. Calculation of image intensities

Because of spherical aberration and defocus of the objective lens of the electron microscope, the magnified image is an imperfect representation of the object structure. The effect of spherical aberration and of defocusing can be represented as modifying the relative phases of the diffracted beams by a phase distortion function $H(s)$, where

$$H(s) = \exp[+i\gamma(s)] \tag{6a}$$

and

$$\gamma(s) = \pi s^2 \lambda (C_s s^2 \lambda^2/2 - \Delta f). \tag{6b}$$

Here, $\gamma(s)$ is the phase distortion factor, s is the spatial frequency, λ is the electron wavelength, C_s is the spherical aberration coefficient and Δf is the amount of defocus.

The image wave function, described as the Fourier transform of the diffracted wave function after modification of phases, can be represented by

$$\psi_i(x,y) = 1 - i\psi_o(x,y) * \mathscr{F}^{-1}[\cos\gamma(s)] + \psi_o(x,y) * \mathscr{F}^{-1}[\sin\gamma(s)], \tag{7}$$

where $\psi_i(x,y)$ is the image wave function and $\psi_o(x,y)$ represents the inverse Fourier transform of the diffracted wave function; $\mathscr{F}^{-1}$ is the inverse Fourier transform operator; $\psi_o(x,y)$ is proportional to the projected potential in the weak phase-object approximation, and in the kinematic approximation $\psi_o(x,y)$ is proportional to the inverse Fourier transform of $F_{\text{kin}}(h,k)$, which is defined in (2).

The image intensity can be described as the product of the image wave function and its complex conjugate. The Fourier coefficients of the image intensity, $\hat{I}(\mathbf{s})$, are obtained by Fourier transformation and can be written as

$$\hat{I}(\mathbf{s}) = \delta(\mathbf{s}) + 2\Phi(h,k)\sin\gamma(\mathbf{s}) + \text{second order terms in } \Phi(h,k), \tag{8}$$

where $\delta(\mathbf{s})$ is the Dirac delta function and $\sin\gamma(\mathbf{s})$ is called the phase-contrast transfer function. The second-order terms can be neglected without resulting in a significant error in the image intensity since, in the single-scattering formulations, $\Phi(h,k)$ is assumed to be very small compared to unity. With such an approximation the projected potential can therefore be retrieved from the image intensity, when all parameters determining the transfer function are known and when the transfer function does not go to zero.

Over a large range of spatial frequencies prescribed by the 'optimum defocus condition' of Scherzer (1949), the transfer function is almost constant. The optimum defocus condition designates the values of defocusing

and of the limiting objective aperture to be (Cowley, 1975)

$$\Delta f = +\tfrac{4}{3}(C_S \lambda)^{1/2}, \qquad (9)$$

$$S_{ap} = 1{\cdot}51 C_S^{-1/4} \lambda^{-3/4},$$

where S_{ap} is the aperture size, Δf and C_S are respectively the optimum defocus value and spherical aberration coefficient of the lens. All image-intensity calculations were restricted to the optimum (Scherzer) condition.

5. The validity domains of the single-scattering approximations

Typical diffracted wave magnitudes and phases for cytosine are shown in Figs. 1–4 as a function of crystal thickness for low- and high-frequency reflections, for the kinematic approximation, the weak phase-object approximation and the 'exact' multislice approximation. The diffracted wave magnitudes and phases for DISOPS show a very similar behavior to that of cytosine, and therefore are not shown here. The

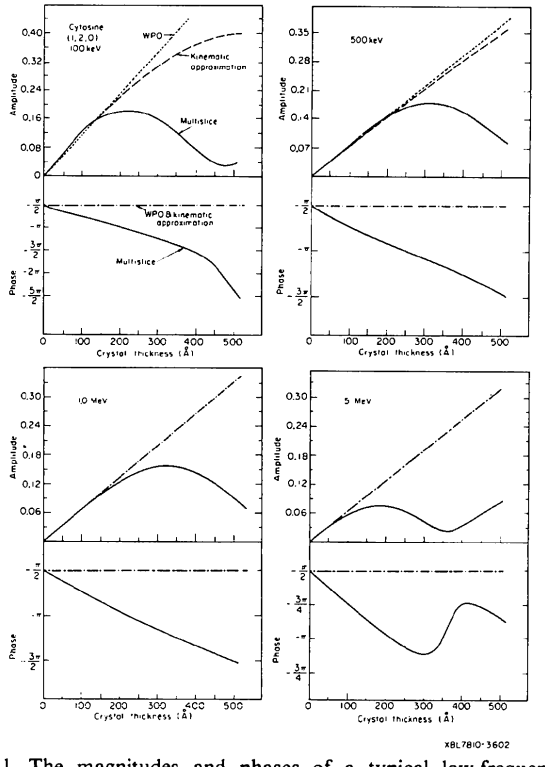

Fig. 1. The magnitudes and phases of a typical low-frequency reflection, (the 120 reflection) of cytosine, calculated using the kinematic approximation (dashed line), the weak phase-object approximation (dotted line), and the multislice formulation (solid line) for thicknesses up to 500 Å, with incident electron energies of 100, 500, 1·0, and 5·0 MeV. The dash-dot line represents both the kinematic and weak phase-object approximation.

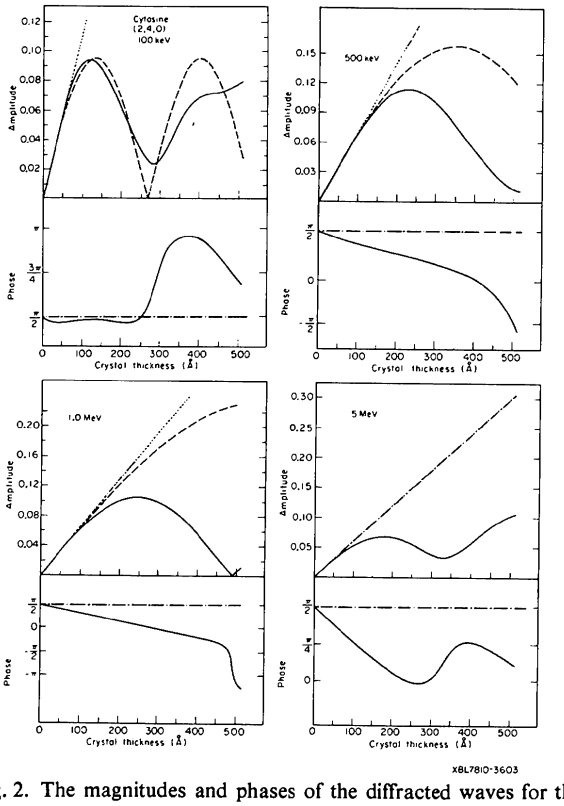

Fig. 2. The magnitudes and phases of the diffracted waves for the 240 reflection; the notation is the same as in Fig. 1.

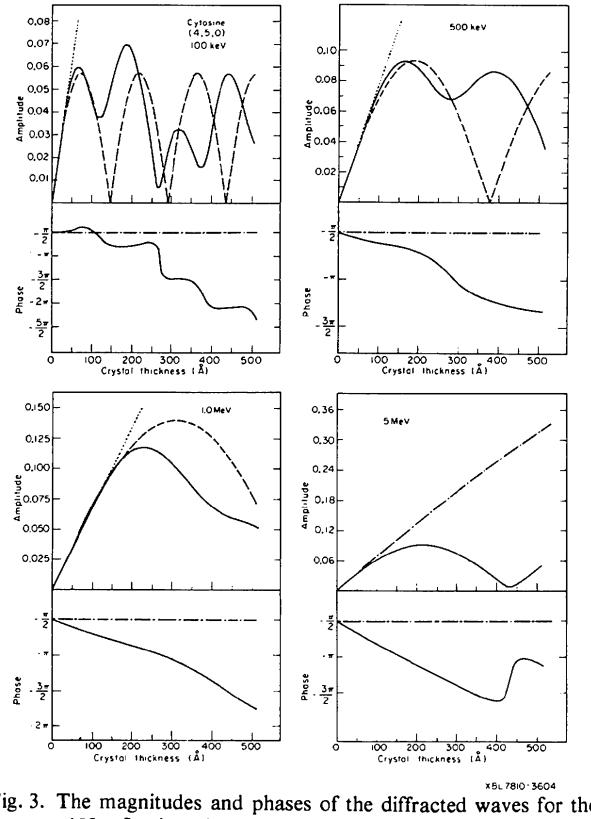

Fig. 3. The magnitudes and phases of the diffracted waves for the 450 reflection; the notation is as described in Fig. 1.

diffracted waves have been computed at various incident electron energies, and they give a qualitative picture of the validity of the approximations in terms of crystal thickness, resolution and electron energy.

The graphs indicate that the domains of validity for the single-scattering approximations are limited to thin crystals. These domains increase when the electron energy is raised to 500 keV, and remain approximately unchanged as the electron energy increases to 1·0 MeV. As the energy is further increased, the domains again decrease. The graphs also indicate that the weak phase-object approximation gives over-estimated values of the amplitudes of the high-frequency reflections at low electron energy, and that the kinematic approximation approaches the weak phase-object approximation as the electron energy increases. This is expected, since the weak phase-object approximation assumes that the Ewald sphere is flat. All reflections in the first Laue zone are therefore assumed to be in the exact Bragg condition simultaneously.

It is worth noting here that the dynamical scattering effect is expected to depend on the Fourier coefficients of the crystal potential, the crystal thickness, the spacings of the reflections, the electron-interaction constant and the curvature of the Ewald sphere. As the electron energy increases the electron-interaction constant decreases and converges to a constant value at very high energies. At the same time the Ewald sphere becomes nearly planar. The decrease in the interaction constant at high voltage has an effect similar to a decrease in the Fourier coefficients of the crystal potential; this can result in an increase in the size of the validity domains of the single-scattering approximations (Jap, 1977). On the other hand, the Ewald sphere intersects a greater number of reciprocal-lattice points as its curvature decreases, resulting in a larger number of reflections being strongly excited, and the dynamical scattering effect is enhanced. The net effect of the decrease in both the electron-interaction constant and the curvature of the Ewald sphere may be expected to increase or decrease the validity domains of the single-scattering approximations, depending on the crystal orientation, crystal unit-cell dimensions and the Fourier coefficients of the crystal potential.

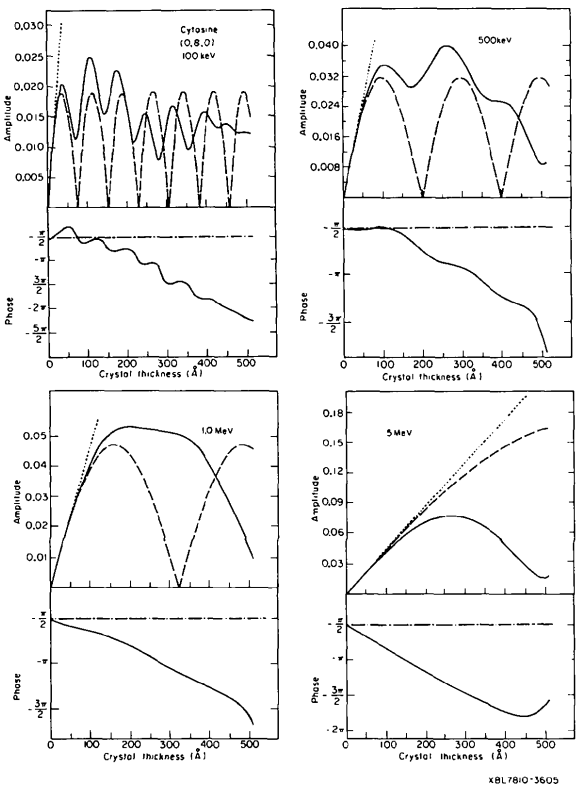

Fig. 4. The magnitudes and phases of the diffracted waves for a typical high-frequency reflection (the 080 reflection); the notation is as described in Fig. 1.

The validity domains of the single-scattering approximations can be more quantitatively assessed on the basis of the agreement of either the diffracted beam amplitudes or the retrieved structure with the corresponding, exact quantities. Two different types of measure are used in this study to establish these validity domains. The first type includes only the amplitudes of the diffracted beams and is therefore useful for comparison to the situation of electron-diffraction studies, where the phase information is not generally available. The second type of measure takes both the phases and amplitudes of the Fourier coefficients of the retrieved, projected potential into consideration. The latter measure can be expected to give a rigorous assessment of the validity of the single-scattering formulations for structural studies in electron microscopy, where both phases and amplitudes of the diffracted beams can in principle be determined.

(*a*) *Electron diffraction*

In a conventional electron diffraction study the validity of a model structure can be established, in part, by comparing the calculated intensities to the experimentally measured intensities. The reliability factor, commonly applied as a quantitative measure for the validity of model structures in X-ray crystallography, has also been used in electron diffraction studies (see, for example, Dorset, 1975; Dorset & Hauptman, 1976; Claffey *et al.*, 1974; Claffey & Blackwell, 1976; Hasegawa, Claffey & Geil, 1977). The numerical value of the reliability factor is liable to change as one increases the maximum spatial frequency included in the summation. In this way the R value defined below can clearly discriminate between the relative agreement of high-resolution and low-resolution information on the model structure.

$$R(s_{\max}) = \sum_{h,k}^{s_{\max}}{}' \big||F_c(h,k)| - N|F_a(h,k)|\big|^2 / \sum_{h,k}^{s_{\max}}{}' |F_c(h,k)|^2 \qquad (10)$$

and

$$N^2 = \sum_{h,k}^{s_{max}}{}' |F_c(h,k)|^2 / \sum_{h,k}^{s_{max}}{}' |F_a(h,k)|^2,$$

where $R(s_{max})$ is the resolution-dependent reliability factor for a maximum spatial frequency, s_{max}; $F_c(h,k)$ and $F_a(h,k)$ are respectively the correct and the approximate diffracted-beam amplitudes with Miller indices (h,k); the prime in the summation means that the (0,0) reflection is excluded; N is a normalization factor. The summation includes only those reflections having spatial frequency less than s_{max}. The validity domains of the single-scattering approximations in terms of resolution, crystal thickness and electron accelerating voltage can be determined for various degrees of reliability, depending on the value assigned to the reliability factor.

The reliability factor for the two single-scattering approximations was calculated for different electron energies in terms of crystal thickness and resolution. In the calculation the 'exact' diffracted beam amplitudes were obtained by the multislice dynamical calculation. There is, of course, no defined value of the reliability factor below which the structure deduced can be considered valid and above which the structure becomes invalid. In X-ray crystallography, it is commonly accepted that the model structure obtained is considered valid and unique when the value of its reliability factor is less than 5%. It is important to note that this does not imply that a structure having a reliability factor slightly greater than 5% should be considered invalid. The validity domains of the single-scattering approximations for electron diffraction analysis at various R values are shown in Fig. 5 in terms of crystal thickness and resolution for various incident electron energies.

Images of the transmitted wave magnitudes calculated with all available diffracted beams for both crystals, cytosine and DISOPS, at 100 keV are displayed in Fig. 6 to provide a qualitative picture of the changes in the transmitted wave magnitudes as the value of the reliability factor varies. Even at a reliability value of 0·05, the transmitted wave magnitudes show a somewhat different appearance from the projected structures, and become increasingly different as the value of the reliability factor increases.

The domains of validity of the single-scattering approximations can be said to be confined to thin crystals and to be limited to increasingly lower

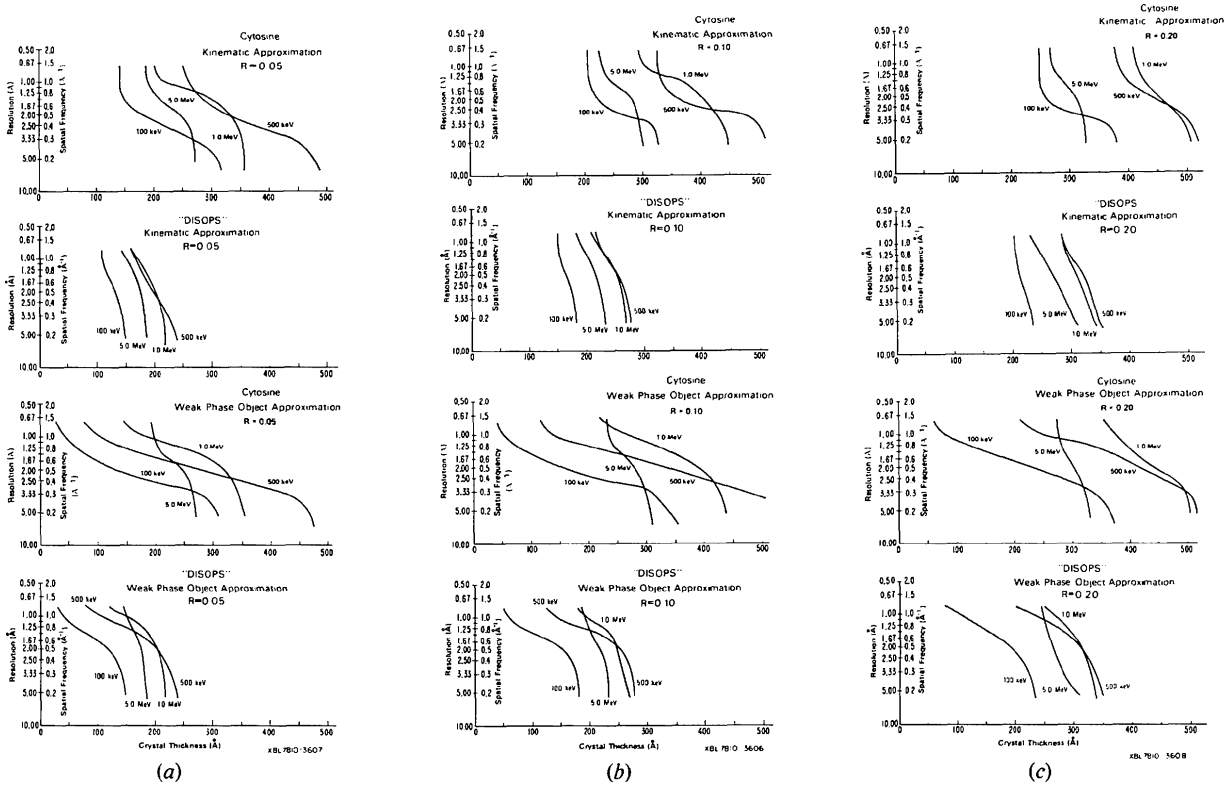

(a) (b) (c)

Fig. 5. (a) The approximate boundary lines at which the diffracted beam magnitudes in the single-scattering approximations possess a reliability factor $R = 0{\cdot}05$. The various curves correspond to different electron incident energy. The two upper graphs represent the kinematic approximation while the lower two are for the weak phase-object approximation. (b) Boundary curves for the domain of validity as described in (a), but for the reliability factor, $R = 0{\cdot}10$. (c) Boundary curves as described in (a) but for the reliability factor, $R = 0{\cdot}20$.

resolution as the crystal thickness increases. As the electron energy is raised to 500 keV, the domains increase. With further increases in electron energy, these domains cease to increase. The validity domains for the crystal DISOPS are confined to smaller areas when compared to those for cytosine, and the dependence of these domains with resolution varies more rapidly as the crystal thickness increases. These effects may result from the fact that DISOPS possesses atoms with 'large' atomic number, namely sodium and sulfur atoms, and from the fact that DISOPS has larger unit-cell dimensions. For a limited spatial frequency, there is an increasing number of reflections involved as the unit-cell dimensions increase. A larger number of beams can therefore be strongly excited in DISOPS, resulting in an increase in the dynamical scattering effect. The increase in the average atomic number also enhances this effect. Consequently, the validity of the single-scattering approximations is confined to a smaller domain.

As the crystal thickness increases, the resolution dependence of the reliability factor in the kinematic approximation varies rapidly, particularly at very high electron energies. In the weak phase-object approximation, the reliability factor changes more gradually with thickness at low electron energy, and at very high electron energies the reliability factor converges to that of the kinematic approximation. At low electron energies the validity of the weak phase-object approximation is confined to a smaller domain compared to that in the kinematic approximation.

It should be noted that the diffracted beam magnitudes in the single-scattering approximations have large deviations from the correct magnitudes computed by the multislice formulation, even for crystal thicknesses at which the reliability factor is small. This apparent inconsistency arises because the reliability factor has been evaluated with diffracted beam magnitudes that were normalized to the 'correct' magnitudes of the multislice formulation. The magnitudes shown in Figs. 1–4 are the 'true' (absolute) values computed by the single-scattering approximations and by the multislice formulation.

(*b*) *Electron microscopy*

Electron microscopy is capable of providing both the amplitude and the phase of the diffracted wave. High-resolution electron microscope images can therefore be used to retrieve the molecular structure directly from the experimental data. The structure so retrieved depends on the formulation used in approximating the physical mapping that occurs between the object structure and diffracted wave. As a measure of validity in this case we have used the dissimilarity factor proposed originally by Linfoot (1956), where the phase as well as the amplitude of the diffracted wave are taken into consideration. The dissimilarity is defined as

$$\mu(s_{\max}) = \sum_{h,k}^{s_{\max}}{}' |F_c(h,k) - F_R(h,k)|^2 / \sum_{h,k}^{s_{\max}}{}' |F_c(h,k)|^2 \quad (11)$$

where $\mu(s_{\max})$ is the dissimilarity factor as a function of the resolution. $F_c(h,k)$ and $F_R(h,k)$ are respectively the Fourier spectrum of the correct and retrieved projected potential, and the prime in the summation indicates that the (0,0) reflection is not included.

The validity of using the single-scattering approximations for the retrieval of the projected potential from the image intensity at the optimum defocus condition was evaluated on the basis of the dissimilarity value. In

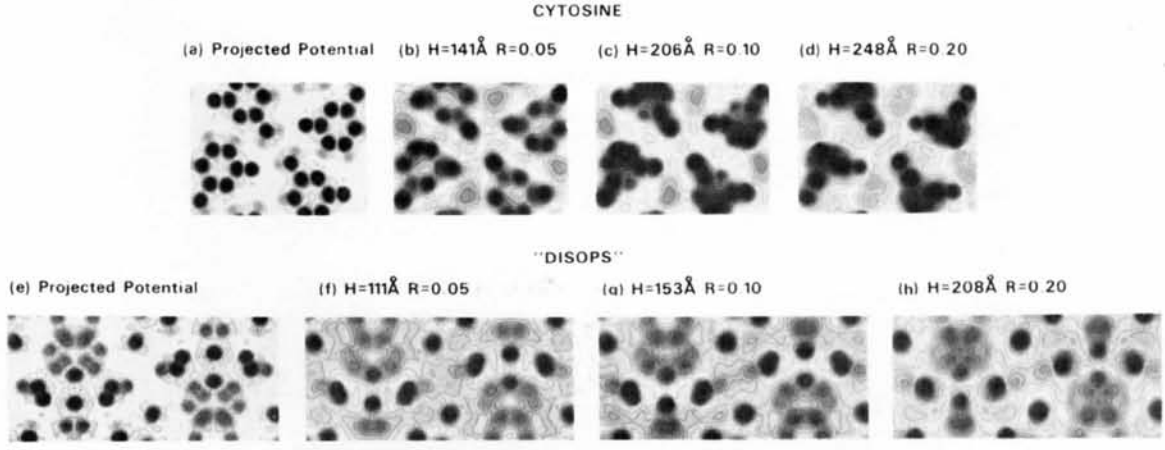

Fig. 6. Half-tone displays of the projected potentials and of the transmitted wave magnitudes for both cytosine and DISOPS at 100 keV. These magnitudes are generated with all diffracted beams available from the calculation (*i.e.* resolution = 0·73 Å for cytosine and 0·80 Å for DISOPS). The increment of the contour levels for the image wave magnitudes was taken to be constant for a given crystal. The contour levels in this case can provide a quantitative picture of the differences in these images. The various images correspond to a thickness, H, at which the diffracted wave magnitudes in the kinematic approximation possess various values of the reliability factor, R, as indicated on the figure.

the evaluation, the Fourier spectrum of the retrieved projected potential was obtained through (8), but ignoring the second-order term. The image intensity was obtained from the 'exact' dynamical diffracted wave and the phase-distortion function. The spherical aberration coefficient was taken to be 0·7 mm at 100 keV, and at higher electron energies it was obtained by keeping $C_S \lambda$ constant.

The validity domains of the two single-scattering approximations (for the retrieval of the projected potential) at different values of the dissimilarity factor are shown in Fig. 7. The overall features of these domains in terms of crystal thickness and resolution are similar to those described previously for the case of electron diffraction. The validity domains for the retrieval of the projected structure are, however, smaller for a given value of both the reliability and dissimilarity factors. This indicates, at thicknesses where the kinematic and the multislice diffracted wave magnitudes are in good agreement, that the correct phases deviate significantly from those expected by the single-scattering approximations and/or that at these thicknesses, the contribution of the second-order term in $F(\mathbf{s})$ to the image intensity cannot be neglected.

The validity domain for the retrieval of the projected potential at 5·0 MeV is larger than the domain at 1·0 MeV, contrary to the results obtained for electron diffraction. This larger domain at 5·0 MeV is to be expected, as the single-scattering approximations exclude the effect of Fresnel propagation through a finite specimen thickness, while the Cowley–Moodie dynamical formulation does not ignore Fresnel propagation. For a given specimen thickness, the effect of Fresnel propagation decreases significantly as the electron energy increases from 1·0 to 5·0 MeV. Consequently, the single-scattering approximations possess a larger domain of validity at 5·0 MeV.

The projected potentials retrieved by the kinematic approximation from the correct image intensities, for various values of the dissimilarity factor at 500 keV,

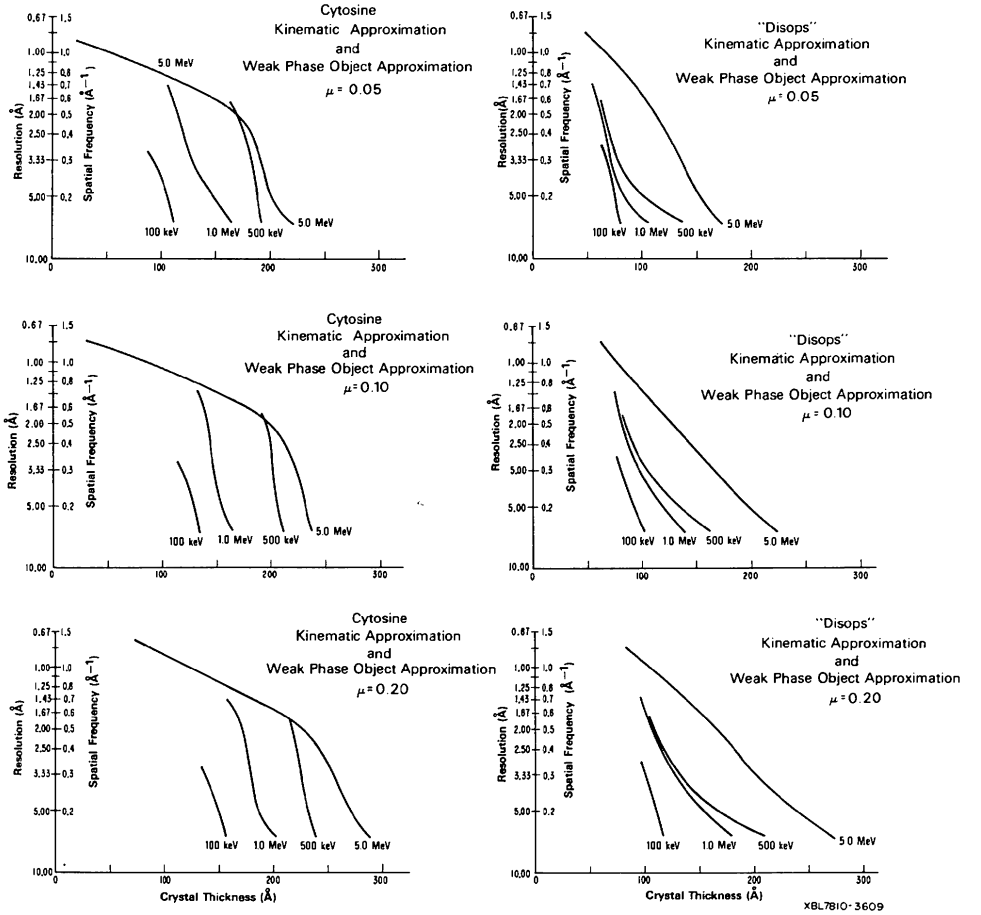

Fig. 7. The approximate boundary lines at which the projected potential retrieved from the dynamical image intensities at optimum defocus condition, by the single-scattering approximations, possess dissimilarity values, $\mu = 0{\cdot}05$, 0·10 and 0·20. The various curves correspond to different electron incident energies.

are displayed in Fig. 8 for both cytosine and DISOPS. The image intensities corresponding to these retrieved, projected potentials are also shown. The retrieved, projected potential is somewhat different from the correct projected potential, even at a dissimilarity value of 0·05, while the image intensity remains qualitatively similar to the projected structure, but with reverse contrast, even when the retrieved projected potential has a large dissimilarity value. This indicates that the phases of the diffracted waves deviate systematically from those expected by the single-scattering approximations in such a way that their image intensity remains similar to the projected structure. The qualitative similarity between the image intensity and the projected structure extends to a larger crystal thickness than is the case for the quantitative validity domains of the single-scattering approximations, if one requires a 'safe' or conservative value of R (reliability) or μ (dissimilarity).

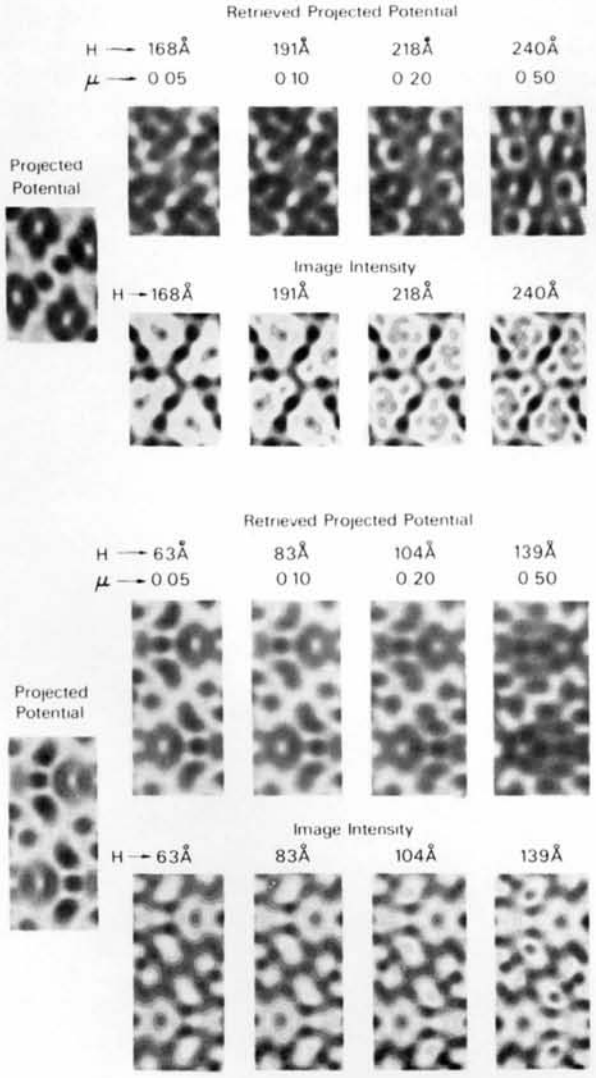

Fig. 8. Half-tone displays of the projected potential of cytosine and of DISOPS; the dynamical image intensities at optimum defocus conditions for crystal thickness H and for electron incident energy 500 keV; and the projected potentials retrieved from those image intensities by the kinematic approximation. All displays have been band limited at a spatial frequency of 0·56 Å^{-1} (*i.e.* a resolution limit of 1·79 Å). The increment of the contour levels was chosen to be constant for the various image intensities and a different constant was used for the retrieved projected potentials. The various projected potentials possess different values of dissimilarity, μ, as indicated.

6. Conclusions and remarks

The domains of validity for the two single-scattering approximations, for quantitative structural analysis of organic crystals, are evaluated in terms of crystal thickness, structural resolution and incident electron energy. For structure determination by electron diffraction, these domains are limited to thin crystals and increase as the electron energy is raised to 500 keV.

For a given crystal structure and crystal orientation, the dynamical scattering effect depends upon the electron-interaction constant and the curvature of the Ewald sphere. The decrease in the interaction constant results in an increase in the size of the validity domain of the single-scattering approximations while the decrease in the curvature of the Ewald sphere often enhances the dynamical scattering effect. The net result of these two factors may either decrease or even increase the domains of validity of the single-scattering approximations.

For organic crystals, the Fourier coefficients of the projected potential decrease rapidly with increasing spatial frequency. Thus a small increase in the number of high-frequency reflections that are strongly excited as the result of a small decrease in the curvature of the Ewald sphere may not significantly alter the small domains of validity of the single-scattering approximations. As the electron energy increases to 500 keV, the validity domains of the single-scattering approximations increase, therefore, by approximately a factor proportional to the decrease in the interaction constant. As the electron energy further increases, the interaction constant decreases *very* slowly while the curvature of the Ewald sphere continues to decrease. The domain of validity first ceases to increase and then decreases as electron energy increases beyond 500 keV.

The validity domains for the retrieval of the projected potential from the image wave function are smaller than those for the case of electron diffraction. The validity domain continues to increase as the electron energy is raised to 5·0 MeV, contrary to results obtained for electron diffraction. The larger domain at 5·0 MeV is not unexpected, as the effect of Fresnel propagation significantly decreases when the electron energy increases from 1·0 to 5·0 MeV.

The dynamical image intensity remains similar to the projected structure, but with reverse contrast, even for a crystal thickness at which the single-scattering approximations fail to provide quantitatively correct, retrieved, projected potentials from the image intensities. The domains in which the image intensity shows a qualitative similarity to the projected structure is larger than those of the single-scattering approximations for the quantitative retrieval of the projected potentials. The use of single-scattering approximations for the retrieval of the projected potential gains, therefore, no additional information over the simple, visual evaluation of the original image intensities.

It is worth noting that the validity domains calculated here are limited to the cases where the potential is projected along a principal crystal axis. The number of reflections, for a limited spatial frequency, is larger than that for a projection that is not parallel to a zone axis. The single-scattering approximations may possess, therefore, larger domains of validity for projections that are not parallel to a zone axis.

The fact that the thickness-resolution domains of validity are quite similar for cytosine and for DISOPS suggests that one might expect the results to be quite generally applicable to other organic structures with similar unit-cell dimensions. Care must be taken, however, that the results should not be assumed to have too great a generality. It is quite likely that organic crystals with smaller cell dimensions than cytosine or DISOPS would have considerably smaller domains of validity for the single-scattering approximations. The relatively small domain of validity of the weak phase-object approximation for graphite (Jefferson, Millward & Thomas, 1976) clearly demonstrates this point. It seems likely that the single-scattering approximations will tend to have a greater validity for large, complex structures than for small, simple structures because it is more likely in the case of small structures that atom centers can overlap in projection. This effect gives rise to large values of the Fourier coefficients of the crystal potential, and a non-linear dependence of the transmitted electron wave function upon the crystal potential. On the other hand, organic structures with much larger unit-cell dimensions will produce a situation in which very many more beams are simultaneously excited than is the case for cytosine or DISOPS. Thus the domain of validity of the single-scattering approximations for larger structures again cannot be accurately predicted from the present results.

Finally, we wish to emphasize that we have not yet explored the effects of any changes in crystal orientation. Thus we cannot predict whether the domains of validity, as they have been defined for the limited diffraction conditions stated above, will also apply to the case of bent crystals.

This work was supported by NIH Grant GM-19452. The authors would like to thank Dr D. Grano for his helpful discussions in the programming and Mr M. H. Ho for his help in submitting some programs.

References

ALLPRESS, J. G., HEWAT, E. A., MOODIE, A. F. & SANDERS, J. V. (1972). *Acta Cryst.* A**28**, 528–536.

BARKER, D. L. & MARSH, R. E. (1964). *Acta Cryst.* **17**, 1581–1587.

CLAFFEY, W. & BLACKWELL, J. (1976). *Biopolymers*, **15**, 1903–1915.

CLAFFEY, W., GARDNER, K., BLACKWELL, J., LANDO, J. & GEIL, P. H. (1974). *Philos. Mag.* **30**, 1223–1232.

COWLEY, J. M. (1975). *Diffraction Physics*, p. 285. Amsterdam: North-Holland/American Elsevier Publishing Company.

COWLEY, J. M. & JAP, B. K. (1976). *9th Annual Scanning Electron Microscopy Meeting* I, edited by OM JOHARI, pp. 377–384.

COWLEY, J. M. & MOODIE, A. F. (1957). *Acta Cryst.* **10**, 609–619.

DORSET, D. L. (1975). *Biochim. Biophys. Acta*, **380**, 257–263.

DORSET, D. L. & HAUPTMAN, H. A. (1976). *Ultramicroscopy*, **1**, 195–201.

DOYLE, P. A. & TURNER, P. S. (1968). *Acta Cryst.* A**24**, 390–397.

ERICKSON, H. P. & KLUG, A. (1971). *Philos. Trans. R. Soc. London Ser. B*, **261**, 105–118.

FRANK, J. (1972). *Biophys. J.* **12**, 484–511.

GOODMAN, J. W. (1968). *Introduction to Fourier Optics Physical and Quantum Electronics Series*, pp. 21–25. New York: McGraw-Hill.

HASEGAWA, H., CLAFFEY, W. & GEIL, P. H. (1977). *J. Macromol. Sci. Phys.* **B13(1)**, 89–100.

HOPPE, W., LANGER, R. & THON, F. (1970). *Optik*, **30**, 538–545.

International Tables for X-ray Crystallography (1968). Vol. II, p. 218. Birmingham: Kynoch Press.

ISHIZUKA, K. & UYEDA, N. (1977). *Acta Cryst.* A**33**, 740–749.

JAP, B. K. (1977). *Phys. Status Solidi A*, **43**, K37–K40.

JAP, B. K. & GLAESER, R. M. (1978). *Acta Cryst.* A**34**, 94–102.

JEFFERSON, D. A., MILLWARD, G. R. & THOMAS, J. M. (1976). *Acta Cryst.* A**32**, 823–828.

LINFOOT, E. (1956). *J. Opt. Soc. Am.* **46**, 740–752.

LYNCH, D. F., MOODIE, A. F. & O'KEEFE, M. A. (1975). *Acta Cryst.* A**31**, 300–307.

SCHERZER, O. (1949). *J. Appl. Phys.* **20**, 20–29.

SLETTEN, J. (1969). *J. Am. Chem. Soc.* **91**, 4545–4549.

STROKE, G. W. & HALIOUA, M. (1973*a*). *Optik*, **37**, 192–203.

STROKE, G. W. & HALIOUA, M. (1973*b*). *Optik*, **37**, 249–264.